AIAA JOURNAL
Vol. 43, No. 7, July 2005

Efficient Reduced-Order System Identification for Linear Systems with Multiple Inputs

Taehyoun Kim*
Boeing Commercial Airplane Group, Seattle, Washington 98124-2207

A new, efficient discrete-time-domain system identification and model reduction method for a large-scaled linear dynamic system with multiple inputs is presented. The method is based on a modification of the classical eigensystem realization algorithm and a simultaneous injection of multiple inputs, so called the single-composite-input method. Because the system response is sampled almost exclusively for the single representative input, this technique can significantly reduce the model construction time as well as the amount of the sampled data. For derivation of the new algorithm, the singular value decomposition is performed using output measurements that are not necessarily attributed to pulse inputs. Application to general computational-fluid-dynamic systems and formulation of reduced-order aeroelastic models are also presented. The efficiency and accuracy of the method is demonstrated via a simple aeroelastic system, which is modeled by the three-dimensional vortex lattice and a six-degrees-of-freedom plate-like structure.

Nomenclature

$\boldsymbol{ABCD}$	=	system matrices
$\boldsymbol{A}_{d1}\boldsymbol{A}_{d2}$	=	aeroelastic system matrices
$\boldsymbol{A}_s\boldsymbol{B}_s\boldsymbol{C}_s$	=	structural system matrices
b	=	reference length
$\boldsymbol{K}$	=	covariance matrix defined in Eq. (42)
L	=	dimension of original system
M	=	number of time or frequency samples
$\boldsymbol{mck}$	=	mass, damping, stiffness matrices
$\boldsymbol{p}$	=	$(R_1 \times 1)$ generalized coordinate vector
q	=	dynamic pressure ($\equiv \frac{1}{2}\rho V^2$)
R	=	number of chosen singular modes or the dimension of realized model
R_1	=	number of chosen Karhunen–Loeve (KL) modes
t	=	real time
$\boldsymbol{u}$	=	$(N_i \times 1)$ input or generalized structural coordinate vector
V	=	air speed
$\boldsymbol{\mathcal{X}}$	=	frequency response of $\boldsymbol{x}$
$\boldsymbol{x}$	=	$(L \times 1)$ state or aerodynamic state vector
$\boldsymbol{y}$	=	$(N_o \times 1)$ output vector or $(N_i \times 1)$ generalized aerodynamic force vector
$\boldsymbol{y}_i$	=	pulse response due to ith input
Δt	=	incremental time step
ρ	=	air density
τ	=	reduced time ($\equiv Vt/b$)
$\boldsymbol{\Phi}$	=	KL modal matrix
ϕ_i	=	KL mode
ω	=	frequency, rad/s
ω_c	=	maximum cutoff frequency

Subscripts

i	=	input
o	=	output
R	=	reduced
ref	=	reference
s	=	structure

Presented as Paper 2004-2036 at the AIAA/ASME/ASCE/AHS/ASC 45th Structures, Structural Dynamics, and Materials Conference, Palm Springs, CA, 19–22 April 2004; received 31 May 2004; revision received 10 January 2005; accepted for publication 16 January 2005.

*Principal Engineer, MS 03-KR, Flutter Engineering and Methods Development; taehyoun.kim@pss.boeing.com. Member AIAA.

Introduction

MOST modern dynamic models are constructed based on finite spatial discretizations of continuous systems, resulting in a considerable number of degrees of freedom in the model. Consequently, for fast and efficient estimation of dynamic behavior as well as optimization and closed-loop control design, a model reduction must be accompanied. Essential requirements for reduced-order dynamic model are that the size of the system must not be too large, the model must be robust and have a good fidelity, it must be in the state-space time-domain formulation for implementation of active control systems and nonlinear time analysis, and finally the reduction process itself must not be too expensive.

There have been many model reduction methods available, but most of them require modifying the main frame of the computational model and are prone to a long model construction time if the model is subjected to many driving inputs. The latter in particular is true in unsteady computational-fluid-dynamic (CFD) applications where the moving solid boundary is often described by many structural mode inputs. For example, a typical Boeing commercial airplane is modeled by as many as 200 structural modes.

Recently, the eigensystem realization algorithm (ERA)[1] was used successfully in application of CFL3D for aeroelastic flutter predictions.[2,3] This method, which is usually used as a system identification technique, has a very attractive feature in that unlike model reduction methods based on the Galerkin scheme[4] there is no need for online implementation of the algorithm. That is, it is a post-processing tool that identifies and generates system matrices based on the input and output data alone. Unfortunately, if the unsteady CFD model is driven by more than one structural input the computation time required to obtain all of the pulse responses increases proportional to the number of the inputs, making the ERA slow and inefficient.

Kim[5] and Kim and Bussoletti[6] introduced the concept of the single-composite-input (SCI) in applications of the Karhunen–Loeve method to unsteady CFD models in the time and frequency domains. The idea herein was that for a linear system one can apply the multiple inputs simultaneously and get all of the system responses that are necessary for the model reduction. Because the computational model needed to be executed only for the representative input, the model construction time was significantly reduced. In this paper, the same approach is adopted for fast and efficient model reduction of linear, finite-dimensional, discrete-time systems.

To accommodate the SCI within the framework of ERA, it is necessary to modify the original algorithm. In particular, the new formulation does not rely on the system Markov parameters explicitly. Instead, it performs the singular value decomposition (SVD) directly on the output measurements that are in general not attributed to pulse inputs. Statistically independent random numbers are used in lieu of the pulses for the multiple input signals. Naturally, the new algorithm can also be used toward system identification provided that all of the time measurements are available from experiments. Application of the SCI/ERA to computational-fluid-dynamic systems and formulation of reduced-order aeroelastic models are also presented.

For a demonstration of the proposed method, an unsteady vortex lattice model in a subsonic, incompressible flow[7] is studied. Reduced-order aeroelastic models are also constructed by combining the reduced aerodynamic models and a plate-like wing that is modeled by six vibrational mode shapes. It is shown that not only the new method reduces the model construction time substantially, but the accuracy of the resulting reduced-order models remains excellent.

The algorithms presented in this paper are a Boeing Intellectual Property and under consideration for a U.S. patent.

Review of Pulse/ERA

In this section, the pulse/ERA (also known as ERA) is reviewed. For simplicity, only its fundamental state-space realization theory, which is attributed to Ho and Kalman,[8] is discussed. For a general description of the method, see Ref. 9. It is assumed that the system under consideration can be described in the following finite-dimensional, discrete-time form:

$$\boldsymbol{x}^{n+1} = \boldsymbol{A}\boldsymbol{x}^n + \boldsymbol{B}\boldsymbol{u}^n \tag{1}$$

$$\boldsymbol{y}^n = \boldsymbol{C}\boldsymbol{x}^n + \boldsymbol{D}\boldsymbol{u}^n \tag{2}$$

where

$$\boldsymbol{x} \equiv (L \times 1) \text{ state vector} \tag{3}$$

$$\boldsymbol{u} \equiv (N_i \times 1) \text{ input vector} \tag{4}$$

$$\boldsymbol{y} \equiv (N_o \times 1) \text{ output vector} \tag{5}$$

The system matrices $(\boldsymbol{A}, \boldsymbol{B})$, $(\boldsymbol{A}, \boldsymbol{C})$ are controllable and observable. First, given $M+1$ equally distributed time steps, $t^n \equiv n\Delta t\,(n = 0, 1, 2, \ldots, M)$, for a single ith input vector the system output is sampled subjected to the unit pulse

$$u_i^n = \delta^n \equiv \begin{Bmatrix} 1 & (n=0) \\ 0 & (n=1, 2, \ldots, M) \end{Bmatrix} \tag{6}$$

Assuming zero initial condition, $\boldsymbol{x}^0 \equiv \boldsymbol{x}(0) = 0$, one obtains

$$\begin{aligned} \boldsymbol{y}_i^0 &= \boldsymbol{d}_i \\ \boldsymbol{y}_i^1 &= \boldsymbol{C}\boldsymbol{b}_i \\ \boldsymbol{y}_i^2 &= \boldsymbol{C}\boldsymbol{A}\boldsymbol{b}_i \\ \boldsymbol{y}_i^3 &= \boldsymbol{C}\boldsymbol{A}^2\boldsymbol{b}_i \\ &\vdots \quad \vdots \\ \boldsymbol{y}_i^M &= \boldsymbol{C}\boldsymbol{A}^{M-1}\boldsymbol{b}_i \end{aligned} \tag{7}$$

where

$$\boldsymbol{b}_i \equiv i\text{th column of } \boldsymbol{B} \tag{8}$$

$$\boldsymbol{d}_i \equiv i\text{th column of } \boldsymbol{D} \tag{9}$$

The constant matrices in the preceding sequence are known as the Markov parameters.[1] This step is repeated N_i times for all inputs creating the sequence of pulse-response matrices:

$$\boldsymbol{Y}^n \equiv \begin{bmatrix} \boldsymbol{y}_1^n & \boldsymbol{y}_2^n & \cdots & \boldsymbol{y}_{N_i}^n \end{bmatrix} \qquad (n = 0, 1, 2, \ldots, M) \tag{10}$$

Next, based on the system Markov parameters define $N_o \times [N_i \times (M-1)]$ Hankel matrices:

$$\begin{aligned} \boldsymbol{H}_0 &\equiv [\boldsymbol{Y}^1 \quad \boldsymbol{Y}^2 \quad \cdots \quad \boldsymbol{Y}^{M-1}] \\ &= \boldsymbol{C}[\boldsymbol{I} \quad \boldsymbol{A} \quad \boldsymbol{A}^2 \quad \cdots \quad \boldsymbol{A}^{M-2}]\boldsymbol{B} \end{aligned} \tag{11}$$

$$\begin{aligned} \boldsymbol{H}_1 &\equiv [\boldsymbol{Y}^2 \quad \boldsymbol{Y}^3 \quad \cdots \quad \boldsymbol{Y}^{M}] \\ &= \boldsymbol{C}[\boldsymbol{A} \quad \boldsymbol{A}^2 \quad \cdots \quad \boldsymbol{A}^{M-1}]\boldsymbol{B} \end{aligned} \tag{12}$$

SVD of $\boldsymbol{H}_0$ yields

$$\begin{aligned} \boldsymbol{H}_0 &\equiv \boldsymbol{U}\boldsymbol{\Sigma}\boldsymbol{V}^T \\ &\simeq [\boldsymbol{U}_R \quad \boldsymbol{U}_D] \begin{bmatrix} \boldsymbol{\Sigma}_R & 0 \\ 0 & 0 \end{bmatrix} \begin{bmatrix} \boldsymbol{V}_R^T \\ \boldsymbol{V}_D^T \end{bmatrix} \\ &= \boldsymbol{U}_R \boldsymbol{\Sigma}_R^{\frac{1}{2}} \boldsymbol{\Sigma}_R^{\frac{1}{2}} \boldsymbol{V}_R^T \end{aligned} \tag{13}$$

where $R \equiv \text{rank}(\boldsymbol{H}_0)$. Finally, a balanced realization of the system under question is obtained by pseudo-inverting various submatrix components as

$$\boldsymbol{D} = \boldsymbol{Y}^0 \quad (N_o \times 1) \tag{14}$$

$$\boldsymbol{C} \simeq \boldsymbol{U}_R \boldsymbol{\Sigma}_R^{\frac{1}{2}} \quad (N_o \times R) \tag{15}$$

$$\boldsymbol{B} \simeq \text{the first } N_i \text{ columns of } \boldsymbol{\Sigma}_R^{\frac{1}{2}} \boldsymbol{V}_R^T \quad (R \times N_i) \tag{16}$$

$$\boldsymbol{A} \simeq \boldsymbol{\Sigma}_R^{-\frac{1}{2}} \boldsymbol{U}_R^T \boldsymbol{H}_1 \boldsymbol{V}_R \boldsymbol{\Sigma}_R^{-\frac{1}{2}} \quad (R \times R) \tag{17}$$

Because $R \ll L$, the preceding model represents a reduced-order realization of the original system. Note that the realization is optimal in that it is balanced between inputs and outputs. However, the total number of samples taken is $N_i \times (M+1)$, which increases proportional to the number of inputs. Also, for an accurate system identification $\boldsymbol{H}_0$ must have sufficient columns and rows, that is, $N_i \times (M-1) \geq R$ and $N_o \geq R$. Figure 1 shows a schematic of the pulse/ERA procedure.

For a very large data set with many time steps and a large number of inputs, the ERA/data correlations (ERA/DC) method is preferred to compress the amount of data and reduce the computation time required for the SVD of the Hankel matrix. See Ref. 1 for details.

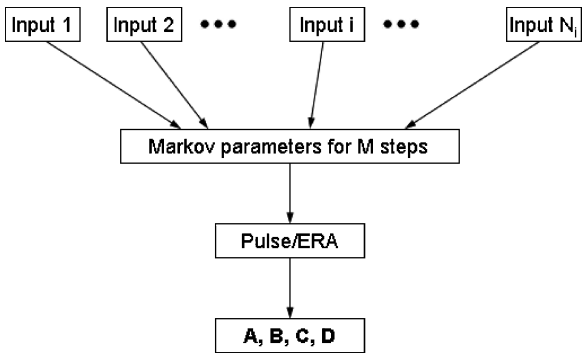

Fig. 1 Schematic of pulse/ERA process.

SCI/ERA

The new method proceeds as follows. First, individual pulse responses are sampled for the first two time steps:

$$\boldsymbol{Y}^0 = \begin{bmatrix} \boldsymbol{y}_1^0 & \boldsymbol{y}_2^0 & \cdots & \boldsymbol{y}_{N_i}^0 \end{bmatrix} \tag{18}$$

$$\boldsymbol{Y}^1 = \begin{bmatrix} \boldsymbol{y}_1^1 & \boldsymbol{y}_2^1 & \cdots & \boldsymbol{y}_{N_i}^1 \end{bmatrix} \tag{19}$$

Next, construct the SCI as

$$\boldsymbol{b}_{\mathrm{SCI}}^n \equiv \sum_{i=1}^{N_i} \boldsymbol{b}_i r_i^n \qquad \text{(for states)} \tag{20}$$

$$\boldsymbol{d}_{\mathrm{SCI}}^n \equiv \sum_{i=1}^{N_i} \boldsymbol{d}_i r_i^n \qquad \text{(for outputs)} \tag{21}$$

where

$$r_i^n \equiv \text{a sequence of arbitrary numbers} \tag{22}$$

To ensure independency of the inputs, one must use signals that are as uncorrelated as possible. Subject to the SCI, we sample the system response $\boldsymbol{y}^n$ for $n = 0, 1, 2, \ldots, M$, and get

$$\begin{aligned} \boldsymbol{y}_{c0}^n &\equiv \boldsymbol{C}\boldsymbol{x}^n \\ &= \boldsymbol{y}^n - \sum_{i=1}^{N_i} \boldsymbol{y}_i^0 r_i^n \end{aligned} \tag{23}$$

$$\begin{aligned} \boldsymbol{y}_{c1}^n &\equiv \boldsymbol{C}\boldsymbol{A}\boldsymbol{x}^n \\ &= \boldsymbol{y}^{n+1} - \sum_{i=1}^{N_i} \boldsymbol{y}_i^0 r_i^{n+1} - \sum_{i=1}^{N_i} \boldsymbol{y}_i^1 r_i^n \end{aligned} \tag{24}$$

Note that $\boldsymbol{y}_{c0}^n, \boldsymbol{y}_{c1}^n$ are measurements of the states in the reduced dimension of $\boldsymbol{C}$ and $\boldsymbol{C}\boldsymbol{A}$. Similar to the Hankel matrices, define

$$\begin{aligned} \boldsymbol{H}_{c0} &\equiv \begin{bmatrix} \boldsymbol{y}_{c0}^1 & \boldsymbol{y}_{c0}^2 & \cdots & \boldsymbol{y}_{c0}^{M-1} \end{bmatrix} \\ &= \boldsymbol{C}[\boldsymbol{x}^1 \quad \boldsymbol{x}^2 \quad \cdots \quad \boldsymbol{x}^{M-1}] \end{aligned} \tag{25}$$

$$\begin{aligned} \boldsymbol{H}_{c1} &\equiv \begin{bmatrix} \boldsymbol{y}_{c1}^1 & \boldsymbol{y}_{c1}^2 & \cdots & \boldsymbol{y}_{c1}^{M-1} \end{bmatrix} \\ &= \boldsymbol{C}\boldsymbol{A}[\boldsymbol{x}^1 \quad \boldsymbol{x}^2 \quad \cdots \quad \boldsymbol{x}^{M-1}] \end{aligned} \tag{26}$$

SVD of $\boldsymbol{H}_{c0}$ yields

$$\begin{aligned} \boldsymbol{H}_{c0} &\equiv \boldsymbol{U}\boldsymbol{\Sigma}\boldsymbol{V}^T \\ &\simeq [\boldsymbol{U}_R \quad \boldsymbol{U}_D] \begin{bmatrix} \boldsymbol{\Sigma}_R & 0 \\ 0 & 0 \end{bmatrix} \begin{bmatrix} \boldsymbol{V}_R^T \\ \boldsymbol{V}_D^T \end{bmatrix} \\ &= \boldsymbol{U}_R \boldsymbol{\Sigma}_R^{\frac{1}{2}} \boldsymbol{\Sigma}_R^{\frac{1}{2}} \boldsymbol{V}_R^T \end{aligned} \tag{27}$$

Once again, $R \equiv \mathrm{rank}(\boldsymbol{H}_{c0})$. The size of the preceding matrices is $N_o \times (M-1)$, N_i times smaller than the previous $\boldsymbol{H}_0, \boldsymbol{H}_1$. The new realization is then

$$\boldsymbol{D} = \boldsymbol{Y}^0 \tag{28}$$

$$\boldsymbol{C} \simeq \boldsymbol{U}_R \boldsymbol{\Sigma}_R^{\frac{1}{2}} \tag{29}$$

$$\boldsymbol{B} \simeq \boldsymbol{\Sigma}_R^{-\frac{1}{2}} \boldsymbol{U}_R^T \boldsymbol{Y}^1 \tag{30}$$

$$\boldsymbol{A} \simeq \boldsymbol{\Sigma}_R^{-\frac{1}{2}} \boldsymbol{U}_R^T \boldsymbol{H}_{c1} \boldsymbol{V}_R \boldsymbol{\Sigma}_R^{-\frac{1}{2}} \tag{31}$$

Unlike the pulse/ERA, the SCI/ERA is optimal in that it is balanced between states and outputs. As in the preceding method, for an accurate realization $\boldsymbol{H}_{c0}$ must have $(M-1) \geq R$ and $N_o \geq R$. However, the total number of samples taken is only $M + 1 + 2 \times N_i$, which is much less than the previous $N_i \times (M+1)$ when M samples of pulse response are taken for each input. Figure 2 shows a schematic of the SCI/ERA procedure.

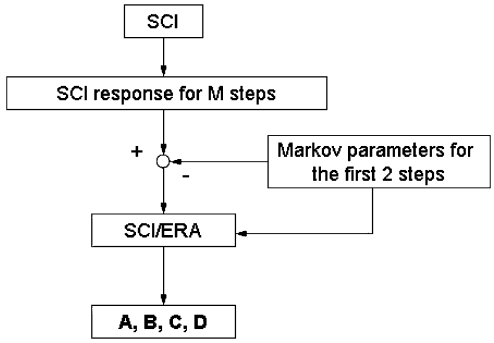

Fig. 2 Schematic of SCI/ERA process.

Two comments regarding the new algorithm are in order. First and foremost, compared with the pulse/ERA the new algorithm requires a much smaller set of time measurements reducing significantly both the computation time and the bulk of the output data. Second, the new $\boldsymbol{H}_{c0}, \boldsymbol{H}_{c1}$ are constructed based on sampled system states subjected to combined random inputs and as such they are not directly related to the Markov parameters. However, the scheme does require the first two pulse responses $\boldsymbol{y}_i^0$ and $\boldsymbol{y}_i^1$ for each input in order to estimate the state measurements based on Eqs. (23) and (24).

Although random signals have been recommended in this paper, other types of signals can also be used for the SCI provided that they are statistically independent. For example, Kim et al.[10] consider SCIs based on low-pass filtered, step, and pulse signals for application of CFL3D for rapid flutter analysis. It is well known that for a linear system any arbitrary response contains the fundamental characteristics under the assumption that the system is controllable and observable. It is this observation, along with the principle of superposition, that the present system identification scheme is based on.

Alternative Scheme with Augmented Measurements

One of the requirements in the ERA methods is that for an accurate model construction a sufficient number of output measurements must be available, more than the number of linearly independent singular modes that are extractable from the Hankel matrices. Failure to satisfy this requirement implies that one does not have enough modes to approximate the system response. When this requirement is not met, assuming again that $(\boldsymbol{A}, \boldsymbol{C})$ is observable we can expand the data matrices by sampling additional responses as follows:

$$\begin{aligned} \boldsymbol{H}_{c01} &\equiv \begin{bmatrix} \boldsymbol{C} \\ \boldsymbol{C}\boldsymbol{A} \\ \boldsymbol{C}\boldsymbol{A}^2 \\ \vdots \\ \boldsymbol{C}\boldsymbol{A}^K \end{bmatrix} [\boldsymbol{x}^1 \quad \boldsymbol{x}^2 \quad \cdots \quad \boldsymbol{x}^{M-1}] \\ &= \begin{bmatrix} \boldsymbol{y}_{c0}^1 & \boldsymbol{y}_{c0}^2 & \cdots & \boldsymbol{y}_{c0}^{M-1} \\ \boldsymbol{y}_{c1}^1 & \boldsymbol{y}_{c1}^2 & \cdots & \boldsymbol{y}_{c1}^{M-1} \\ \cdots & \cdots & \cdots & \cdots \\ \boldsymbol{y}_{\mathrm{cK}}^1 & \boldsymbol{y}_{\mathrm{cK}}^2 & \cdots & \boldsymbol{y}_{\mathrm{cK}}^{M-1} \end{bmatrix} \end{aligned} \tag{32}$$

$$\begin{aligned} \boldsymbol{H}_{c11} &\equiv \begin{bmatrix} \boldsymbol{C} \\ \boldsymbol{C}\boldsymbol{A} \\ \boldsymbol{C}\boldsymbol{A}^2 \\ \vdots \\ \boldsymbol{C}\boldsymbol{A}^K \end{bmatrix} \boldsymbol{A}[\boldsymbol{x}^1 \quad \boldsymbol{x}^2 \quad \cdots \quad \boldsymbol{x}^{M-1}] \\ &= \begin{bmatrix} \boldsymbol{y}_{c1}^1 & \boldsymbol{y}_{c1}^2 & \cdots & \boldsymbol{y}_{c1}^{M-1} \\ \boldsymbol{y}_{c2}^1 & \boldsymbol{y}_{c2}^2 & \cdots & \boldsymbol{y}_{c2}^{M-1} \\ \cdots & \cdots & \cdots & \cdots \\ \boldsymbol{y}_{\mathrm{cK}+1}^1 & \boldsymbol{y}_{\mathrm{cK}+1}^2 & \cdots & \boldsymbol{y}_{\mathrm{cK}+1}^{M-1} \end{bmatrix} \end{aligned} \tag{33}$$

where

$$\begin{aligned} \boldsymbol{y}_{\mathrm{ck}}^{n} &\equiv \boldsymbol{C}\boldsymbol{A}^{k}\boldsymbol{x}^{n} \\ &= \boldsymbol{y}^{n+k} - \sum_{i=1}^{N_i} \boldsymbol{y}_i^0 r_i^{n+k} - \sum_{i=1}^{N_i} \boldsymbol{y}_i^1 r_i^{n+k-1} - \cdots - \sum_{i=1}^{N_i} \boldsymbol{y}_i^k r_i^n \\ &= \boldsymbol{y}^{n+k} - \sum_{j=1}^{k+1} \sum_{i=1}^{N_i} \boldsymbol{y}_i^{j-1} r_i^{n+k+1-j} \quad (k=0,1,2,\ldots,K+1) \end{aligned} \tag{34}$$

SVD of the new $\boldsymbol{H}_{c0}$ leads to

$$\begin{aligned} \boldsymbol{H}_{c01} &\equiv \boldsymbol{U}_1 \boldsymbol{\Sigma}_1 \boldsymbol{V}_1^T \\ &\simeq [\boldsymbol{U}_{1R} \quad \boldsymbol{U}_{1D}] \begin{bmatrix} \boldsymbol{\Sigma}_{1R} & 0 \\ 0 & 0 \end{bmatrix} \begin{bmatrix} \boldsymbol{V}_{1R}^T \\ \boldsymbol{V}_{1D}^T \end{bmatrix} \\ &= \boldsymbol{U}_{1R} \boldsymbol{\Sigma}_{1R}^{\frac{1}{2}} \boldsymbol{\Sigma}_{1R}^{\frac{1}{2}} \boldsymbol{V}_{1R}^T \end{aligned} \tag{35}$$

from which we obtain

$$\boldsymbol{D} = \text{the first } N_o \text{ rows of } \boldsymbol{Y}_c^0 \tag{36}$$

$$\boldsymbol{C} \simeq \text{the first } N_o \text{ rows of } \boldsymbol{U}_{1R} \boldsymbol{\Sigma}_{1R}^{\frac{1}{2}} \tag{37}$$

$$\boldsymbol{B} \simeq \boldsymbol{\Sigma}_{1R}^{-\frac{1}{2}} \boldsymbol{U}_{1R}^T \boldsymbol{Y}_c^1 \tag{38}$$

$$\boldsymbol{A} \simeq \boldsymbol{\Sigma}_{1R}^{-\frac{1}{2}} \boldsymbol{U}_{1R}^T \boldsymbol{H}_{c11} \boldsymbol{V}_{1R} \boldsymbol{\Sigma}_{1R}^{-\frac{1}{2}} \tag{39}$$

where

$$\boldsymbol{Y}_c^n \equiv \begin{bmatrix} \boldsymbol{y}_1^n & \boldsymbol{y}_2^n & \cdots & \boldsymbol{y}_{N_i}^n \\ \boldsymbol{y}_1^{n+1} & \boldsymbol{y}_2^{n+1} & \cdots & \boldsymbol{y}_{N_i}^{n+1} \\ \cdots & \cdots & \cdots & \cdots \\ \boldsymbol{y}_1^{n+K+1} & \boldsymbol{y}_2^{n+K+1} & \cdots & \boldsymbol{y}_{N_i}^{n+K+1} \end{bmatrix} \quad (n=0,1) \tag{40}$$

The total number of measurements available is now $(K+1) \times N_o$. The additional time samples are required for the pulse response as well as for the response caused by the SCI. More specifically, if K blocks of outputs are to be added pulse responses from each input must be sampled at K additional time steps in addition the first two time steps, $t=0$ and Δt. Also, the response from the SCI must be sampled at K additional steps beyond the Mth step. The total number of samples to be taken is thus $M+1+K+(2+K) \times N_i$. K must be sufficiently large enough to satisfy the measurement requirement, $(K+1) \times N_o \geq R$. Needless to say, this scheme requires extra computation time because of the additional time samples required in the data set.

Second Reduction Based on Frequency-Domain Karhunen–Loeve/SCI Method

In applications of discrete-time computational models, there exist two conflicting requirements for the incremental time step Δt. For numerical convergence one has to adopt a sufficiently small Δt_1. On the other hand, given the highest frequency of interest ω_c Nyquist criterion requires $\Delta t_2 \leq \pi/\omega_c$. Usually, for practical purposes $\Delta t_2 \gg \Delta t_1$. For instance, in a structural model that is coupled with a CFD model for aeroelastic applications the highest mode usually has a much lower natural frequency than the highest frequency content in the aerodynamic model. If the input signals used in the ERA methods are sharp as in the random, step, or pulse inputs, the SCI will excite all of the system dynamics, and hence this characteristic will be carried over to the ERA-based reduced-order model. As a result, the ERA reduced-order model (ROM) is prone to have a large dimension to span the same high-frequency range as the original full-order model (FOM), which suggests that there might be room for further order reduction in the ROM. To perform a second-order reduction, one can apply the frequency-domain Karhunen–Loeve (FDKL) procedure[11] to the ERA ROM obtained by matrices (28–31) wherein frequency samples of the system within a given frequency range $(-\omega_c, \omega_c)$ are used to extract optimal modes, and a new reduced-order model is constructed via the Galerkin's approximation. According to the method, the optimal or so-called KL modes ϕ_i are the eigenmodes of the covariance matrix $\boldsymbol{K}$:

$$\boldsymbol{K}\phi_i = \lambda_i \phi_i \tag{41}$$

where

$$K_{ij} \equiv \boldsymbol{\mathcal{X}}(\omega_i) \boldsymbol{\mathcal{X}}(\omega_j)^{*T} \tag{42}$$

$$\begin{aligned} \omega_i &\equiv \text{sampling frequencies} \\ &= [\omega_1 \quad \omega_2 \quad \cdots \quad \omega_M] \end{aligned} \tag{43}$$

where $\omega_1 = -\omega_c$ and $\omega_M = \omega_c$. To facilitate the SCI in the frequency domain, $\boldsymbol{\mathcal{X}}_i(\omega_i)$ are sampled subjected to the same input described by Eq. (20) and (21) but with the understanding that these random numbers have been generated in the frequency domain.[12] Another feature of this FDKL/SCI method is that the number of the sampling frequencies is optimized by beginning with just three sample points at $0, \omega_c/2, \omega_c$, and continuously updating the rank of the covrariance matrix at each additional sample point. The sampling automatically stops when the rank is converged.

Once the optimal modes are obtained, assume

$$\boldsymbol{x} \simeq \boldsymbol{\Phi}\boldsymbol{p} \tag{44}$$

where

$$\boldsymbol{\Phi} \equiv \begin{bmatrix} \phi_1 & \phi_2 & \cdots & \phi_{R_1} \end{bmatrix} \tag{45}$$

$$\boldsymbol{p} \equiv \begin{Bmatrix} p_1 \\ p_2 \\ \vdots \\ p_{R_1} \end{Bmatrix} \tag{46}$$

R_1 is set to be equal to the rank of the covariance matrix, which is usually smaller than R. After inserting Eq. (44) into Eqs. (1) and (2) with the ERA ROM matrices, premultiplying both sides by $\boldsymbol{\Phi}^T$ yields a new reduced-order model as

$$\boldsymbol{p}^{n+1} = \boldsymbol{A}_1 \boldsymbol{p}^n + \boldsymbol{B}_1 \boldsymbol{u}^n \tag{47}$$

$$\boldsymbol{y}^n = \boldsymbol{C}_1 \boldsymbol{p}^n + \boldsymbol{D}\boldsymbol{u}^n \tag{48}$$

where

$$\boldsymbol{A}_1 \equiv \boldsymbol{\Phi}^T \boldsymbol{A} \boldsymbol{\Phi} \tag{49}$$

$$\boldsymbol{B}_1 \equiv \boldsymbol{\Phi}^T \boldsymbol{B} \tag{50}$$

$$\boldsymbol{C}_1 \equiv \boldsymbol{C}\boldsymbol{\Phi} \tag{51}$$

The dimension of the new model is $(R_1 \times R_1)$.

Application to CFD Model

In this section, application of the proposed model reduction/system identification method to large-scaled CFD models is discussed. Unlike the general system described by Eqs. (1) and (2), an unsteady fluid dynamic system is driven by displacement and velocity of its moving boundary surface simultaneously as they both contribute to the normal downwash on the surface. If one considers a statically nonlinear, dynamically linearized flowfield, the unsteady fluid motion can be described as

$$\boldsymbol{x}^{n+1} = \boldsymbol{A}\boldsymbol{x}^n + \boldsymbol{B}_0 \boldsymbol{u}^n + \boldsymbol{B}_1 \dot{\boldsymbol{u}}^n \tag{52}$$

$$\boldsymbol{y}^n = q\left(\boldsymbol{C}\boldsymbol{x}^n + \boldsymbol{D}_0 \boldsymbol{u}^n + \boldsymbol{D}_1 \dot{\boldsymbol{u}}^n\right) \tag{53}$$

where

$$\boldsymbol{x} \equiv (L \times 1) \text{ fluid states} \tag{54}$$

$$\boldsymbol{u} \equiv (N_i \times 1) \text{ generalized displacements} \tag{55}$$

$$\dot{\boldsymbol{u}} \equiv (N_i \times 1) \text{ generalized velocities} \tag{56}$$

$$\boldsymbol{y} \equiv (N_i \times 1) \text{ generalized aerodynamic forces} \tag{57}$$

The preceding equations progress in nondimensional time, $\tau \equiv Vt/b$, rather than in the real time t and $(\dot{})$ is the first derivative with respect to τ. In fact, the dependency of the normal downwash on air speed disappears when the equations are discretized in τ, as in Eqs. (52) and (53). The structural degrees of freedom u_i are the generalized coordinates associated with structural modes. These modes are used to describe the motion of the lifting surface. Two different types of reduced-order fluid dynamic models can be obtained depending on how the inputs are treated. If necessary, the FDKL/SCI can be performed for an additional reduction.

Aerodynamic ROM with Displacement and Velocity Inputs

One can treat $\boldsymbol{u}^n$ and $\dot{\boldsymbol{u}}^n$ separately as independent inputs. Thus, for the pulse inputs

$$u_i^n = \dot{u}_i^n = \delta^n \equiv \begin{Bmatrix} 1 & (n=0) \\ 0 & (n=1,2,\ldots,M) \end{Bmatrix} \tag{58}$$

for $i = 1, 2, \ldots, N_i$, we obtain the corresponding responses $\boldsymbol{y}_i^0, \boldsymbol{y}_i^1$ at the first two time steps. Let us define

$$\boldsymbol{Y}^0 = \begin{bmatrix} \boldsymbol{y}_1^0 & \boldsymbol{y}_2^0 & \cdots & \boldsymbol{y}_{N_i}^0 & \boldsymbol{y}_{N_i+1}^0 & \boldsymbol{y}_{N_i+2}^0 & \cdots & \boldsymbol{y}_{2N_i}^0 \end{bmatrix} \tag{59}$$

$$\boldsymbol{Y}^1 = \begin{bmatrix} \boldsymbol{y}_1^1 & \boldsymbol{y}_2^1 & \cdots & \boldsymbol{y}_{N_i}^1 & \boldsymbol{y}_{N_i+1}^1 & \boldsymbol{y}_{N_i+2}^1 & \cdots & \boldsymbol{y}_{2N_i}^1 \end{bmatrix} \tag{60}$$

where the first N_i samples are because of the pulses in $\boldsymbol{u}^n$ and the next N_i ones are because of the pulses in $\dot{\boldsymbol{u}}^n$. Next, we prepare the following inputs:

$$\boldsymbol{b}_{\text{SCI}}^n \equiv \sum_{i=1}^{N_i} \boldsymbol{b}_{0i} r_i^n + \sum_{i=1}^{N_i} \boldsymbol{b}_{1i} r_{N_i+i}^n \tag{61}$$

$$\boldsymbol{d}_{\text{SCI}}^n \equiv \sum_{i=1}^{N_i} \boldsymbol{d}_{0i} r_i^n + \sum_{i=1}^{N_i} \boldsymbol{d}_{1i} r_{N_i+i}^n \tag{62}$$

Subject to the SCI, we sample the system response $\boldsymbol{y}^n$ and get

$$\boldsymbol{y}_{c0}^n \equiv \boldsymbol{y}^n - \sum_{i=1}^{2N_i} \boldsymbol{y}_i^0 r_i^n \tag{63}$$

$$\boldsymbol{y}_{c1}^n \equiv \boldsymbol{y}^{n+1} - \sum_{i=1}^{2N_i} \boldsymbol{y}_i^0 r_i^{n+1} - \sum_{i=1}^{2N_i} \boldsymbol{y}_i^1 r_i^n \tag{64}$$

Define

$$\boldsymbol{H}_{c0} \equiv \begin{bmatrix} \boldsymbol{y}_{c0}^1 & \boldsymbol{y}_{c0}^2 & \cdots & \boldsymbol{y}_{c0}^{M-1} \end{bmatrix} \tag{65}$$

$$\boldsymbol{H}_{c1} \equiv \begin{bmatrix} \boldsymbol{y}_{c1}^1 & \boldsymbol{y}_{c1}^2 & \cdots & \boldsymbol{y}_{c1}^{M-1} \end{bmatrix} \tag{66}$$

where SVD of $\boldsymbol{H}_{c0}$ yields

$$\begin{aligned} \boldsymbol{H}_{c0} &\equiv \boldsymbol{U}\boldsymbol{\Sigma}\boldsymbol{V}^T \\ &\simeq \begin{bmatrix} \boldsymbol{U}_R & \boldsymbol{U}_D \end{bmatrix} \begin{bmatrix} \boldsymbol{\Sigma}_R & 0 \\ 0 & 0 \end{bmatrix} \begin{bmatrix} \boldsymbol{V}_R^T \\ \boldsymbol{V}_D^T \end{bmatrix} \\ &= \boldsymbol{U}_R \boldsymbol{\Sigma}_R^{\frac{1}{2}} \boldsymbol{\Sigma}_R^{\frac{1}{2}} \boldsymbol{V}_R^T \end{aligned} \tag{67}$$

with $R \equiv \text{rank}(\boldsymbol{H}_{c0})$. Hence, the reduced-order model is given by

$$\boldsymbol{D}_0 = \text{the first } N_i \text{ columns of } \boldsymbol{Y}^0 \tag{68}$$

$$\boldsymbol{D}_1 = \text{the second } N_i \text{ columns of } \boldsymbol{Y}^0 \tag{69}$$

$$\boldsymbol{C} \simeq \boldsymbol{U}_R \boldsymbol{\Sigma}_R^{\frac{1}{2}} \tag{70}$$

$$\boldsymbol{B}_0 \simeq \text{the first } N_i \text{ columns of } \boldsymbol{\Sigma}_R^{-\frac{1}{2}} \boldsymbol{U}_R^T \boldsymbol{Y}^1 \tag{71}$$

$$\boldsymbol{B}_1 \simeq \text{the second } N_i \text{ columns of } \boldsymbol{\Sigma}_R^{-\frac{1}{2}} \boldsymbol{U}_R^T \boldsymbol{Y}^1 \tag{72}$$

$$\boldsymbol{A} \simeq \boldsymbol{\Sigma}_R^{-\frac{1}{2}} \boldsymbol{U}_R^T \boldsymbol{H}_{c1} \boldsymbol{V}_R \boldsymbol{\Sigma}_R^{-\frac{1}{2}} \tag{73}$$

Aerodynamic ROM with Displacement Inputs

The second scheme is to use only the displacements as the system inputs. This is possible by applying simultaneously the pulse and double pulse inputs,

$$u_i^n = \delta^n \equiv \begin{Bmatrix} 1 & (n=0) \\ 0 & (n=1,2,\ldots,M) \end{Bmatrix} \tag{74}$$

$$\dot{u}_i^n = \dot{\delta}^n \equiv \begin{Bmatrix} \dfrac{1}{\Delta\tau} & (n=0) \\ -\dfrac{1}{\Delta\tau} & (n=1) \\ 0 & (n=2,3,\ldots,M) \end{Bmatrix} \tag{75}$$

and get the corresponding responses $\boldsymbol{y}_{\text{di}}^0, \boldsymbol{y}_{\text{di}}^1$ at the first two time steps:

$$\boldsymbol{Y}_d^0 = \begin{bmatrix} \boldsymbol{y}_{d1}^0 & \boldsymbol{y}_{d2}^0 & \cdots & \boldsymbol{y}_{\text{dN}_i}^0 \end{bmatrix} \tag{76}$$

$$\boldsymbol{Y}_d^1 = \begin{bmatrix} \boldsymbol{y}_{d1}^1 & \boldsymbol{y}_{d2}^1 & \cdots & \boldsymbol{y}_{\text{dN}_i}^1 \end{bmatrix} \tag{77}$$

For the SCI, we use

$$\boldsymbol{b}_{\text{SCI}}^n \equiv \sum_{i=1}^{N_i} \boldsymbol{b}_{0i} r_i^n + \sum_{i=1}^{N_i} \boldsymbol{b}_{1i} \dot{r}_i^n \tag{78}$$

$$\boldsymbol{d}_{\text{SCI}}^n \equiv \sum_{i=1}^{N_i} \boldsymbol{d}_{0i} r_i^n + \sum_{i=1}^{N_i} \boldsymbol{d}_{1i} \dot{r}_i^n \tag{79}$$

where $\dot{r}_i^n$ is the discrete-time derivative of r_i^n. To be consistent with the use of the double pulse defined in Eq. (75), $\dot{r}_i^n$ is obtained by filtering r_i^n via $\dot{\delta}_i^n$, that is,

$$\dot{r}_i^n \equiv \text{conv}\left(r_i^k, \dot{\delta}_i^k\right) \tag{80}$$

which is equivalent to the backward difference equation,

$$\dot{r}_i^n \equiv \frac{r_i^n - r_i^{n-1}}{\Delta\tau} \tag{81}$$

Subject to the new SCI, we sample the system response $\boldsymbol{y}^n$ and get

$$\boldsymbol{y}_{\text{dc0}}^n \equiv \boldsymbol{y}^n - \sum_{i=1}^{N_i} \boldsymbol{y}_{\text{di}}^0 r_i^n \tag{82}$$

$$\boldsymbol{y}_{\text{dc1}}^n \equiv \boldsymbol{y}^{n+1} - \sum_{i=1}^{N_i} \boldsymbol{y}_{\text{di}}^0 r_i^{n+1} - \sum_{i=1}^{N_i} \boldsymbol{y}_{\text{di}}^1 r_i^n \tag{83}$$

Defining

$$\boldsymbol{H}_{\text{dc0}} \equiv \begin{bmatrix} \boldsymbol{y}_{\text{dc0}}^1 & \boldsymbol{y}_{\text{dc0}}^2 & \cdots & \boldsymbol{y}_{\text{dc0}}^{M-1} \end{bmatrix} \tag{84}$$

$$\boldsymbol{H}_{\text{dc1}} \equiv \begin{bmatrix} \boldsymbol{y}_{\text{dc1}}^1 & \boldsymbol{y}_{\text{dc1}}^2 & \cdots & \boldsymbol{y}_{\text{dc1}}^{M-1} \end{bmatrix} \tag{85}$$

the SVD of $\boldsymbol{H}_{\mathrm{dc0}}$ yields

$$\boldsymbol{H}_{\mathrm{dc0}} \equiv \boldsymbol{U}\boldsymbol{\Sigma}\boldsymbol{V}^T \simeq [\boldsymbol{U}_R \quad \boldsymbol{U}_D]\begin{bmatrix}\boldsymbol{\Sigma}_R & 0\\ 0 & 0\end{bmatrix}\begin{bmatrix}\boldsymbol{V}_R^T\\ \boldsymbol{V}_D^T\end{bmatrix} = \boldsymbol{U}_R\boldsymbol{\Sigma}_R^{\frac{1}{2}}\boldsymbol{\Sigma}_R^{\frac{1}{2}}\boldsymbol{V}_R^T \tag{86}$$

with $R \equiv \mathrm{rank}(\boldsymbol{H}_{\mathrm{dc0}})$. The new reduced-order model has only N_i input channels and is in the form

$$\boldsymbol{x}^{n+1} = \boldsymbol{A}\boldsymbol{x}^n + \boldsymbol{B}\boldsymbol{u}^n \tag{87}$$

$$\boldsymbol{y}^n = q(\boldsymbol{C}\boldsymbol{x}^n + \boldsymbol{D}\boldsymbol{u}^n) \tag{88}$$

where

$$\boldsymbol{D} = \boldsymbol{Y}_d^0 \tag{89}$$

$$\boldsymbol{C} \simeq \boldsymbol{U}_R\boldsymbol{\Sigma}_R^{\frac{1}{2}} \tag{90}$$

$$\boldsymbol{B} \simeq \boldsymbol{\Sigma}_R^{-\frac{1}{2}}\boldsymbol{U}_R^T\boldsymbol{Y}_d^1 \tag{91}$$

$$\boldsymbol{A} \simeq \boldsymbol{\Sigma}_R^{-\frac{1}{2}}\boldsymbol{U}_R^T\boldsymbol{H}_{\mathrm{dc1}}\boldsymbol{V}_R\boldsymbol{\Sigma}_R^{-\frac{1}{2}} \tag{92}$$

Reduced-Order Aeroelastic Model

We illustrate how aeroelastic systems can be constructed using the reduced-order aerodynamic models obtained in the preceding section.

First, we note that structural model is normally described in the real, continuous time

$$\boldsymbol{m}\ddot{\boldsymbol{u}} + \boldsymbol{c}\dot{\boldsymbol{u}} + \boldsymbol{k}\boldsymbol{u} = \boldsymbol{y} \tag{93}$$

$(\dot{})$ and $(\ddot{})$, respectively, represent the first and the second derivatives with respect to t. Hence, to construct aeroelastic model the continuous-time equation (93) is discretized in time:

$$\boldsymbol{z}^{n+1} = \boldsymbol{A}_s\boldsymbol{z}^n + \boldsymbol{B}_s\boldsymbol{y}^n \tag{94}$$

$$\boldsymbol{u}^n = \boldsymbol{C}_s\boldsymbol{z}^n \tag{95}$$

where

$$\boldsymbol{z} \equiv \begin{Bmatrix}\boldsymbol{u}\\ \dot{\boldsymbol{u}}\end{Bmatrix} \tag{96}$$

$$\boldsymbol{C}_s \equiv [\boldsymbol{I} \quad 0] \tag{97}$$

Note that given $\Delta\tau$ and V the consistent incremental time step, $\Delta t = \Delta\tau b/V$, must be used in the conversion to the discrete time.

Aeroelastic Model I

In this approach, we treat $\boldsymbol{u}^n, \dot{\boldsymbol{u}}^n$ as independent inputs and apply the $\boldsymbol{b}_{\mathrm{SCI}}^n, \boldsymbol{d}_{\mathrm{SCI}}^n$ given by Eqs. (61) and (62) at a reference dynamic pressure q_{ref}. The corresponding samples are taken and scaled by $1/q_{\mathrm{ref}}$. The aerodynamic ROM of the first kind described earlier is then obtained by applying the SCI/ERA. An aeroelastic system that is valid at all air speeds can be constructed by combining the resulting aerodynamic ROM with the structural equations:

$$\boldsymbol{X}^{n+1} = \boldsymbol{A}_{d1}\boldsymbol{X}^n \tag{98}$$

where

$$\boldsymbol{X} \equiv \begin{Bmatrix}\boldsymbol{x}\\ \boldsymbol{z}\end{Bmatrix} \tag{99}$$

$$\boldsymbol{A}_{d1} \equiv \begin{bmatrix}\boldsymbol{A} & [\boldsymbol{B}_0 \quad \boldsymbol{B}_1]\\ q\boldsymbol{B}_s\boldsymbol{C} & \boldsymbol{A}_s + q\boldsymbol{B}_s[\boldsymbol{D}_0 \quad \boldsymbol{D}_1]\end{bmatrix} \tag{100}$$

Denoting the eigenvalues of system matrix (100) as λ_{d1i}, the aeroelastic eigenvalues in the Laplace domain are obtained as

$$\lambda_{c1i} = \log(\lambda_{d1i})/\Delta t \tag{101}$$

For flutter instability, one must have $\mathrm{Real}(\lambda_{c1i}) > 0$ and $\|\lambda_{d1i}\| > 1$ for any i.

Aeroelastic Model II

One can also apply the $\boldsymbol{b}_{\mathrm{SCI}}^n, \boldsymbol{d}_{\mathrm{SCI}}^n$ given by Eqs. (78) and (79) and get the aerodynamic ROM of the second kind, Eqs. (87) and (88). The new resulting reduced-order aeroelastic model is obtained as

$$\boldsymbol{X}^{n+1} = \boldsymbol{A}_{d2}\boldsymbol{X}^n \tag{102}$$

where

$$\boldsymbol{A}_{d2} \equiv \begin{bmatrix}\boldsymbol{A} & \boldsymbol{B}\boldsymbol{C}_s\\ q\boldsymbol{B}_s\boldsymbol{C} & \boldsymbol{A}_s + q\boldsymbol{B}_s\boldsymbol{D}\boldsymbol{C}_s\end{bmatrix} \tag{103}$$

Although q can change in Eq. (103), this model must be restricted to the reference air speed V_{ref}. It is well known that the total downwash on the moving boundary depends on both the displacement u and velocity $\dot{u}$, and as such it is impossible to separate out and account for the effect of V with the displacement channel alone. However, this drawback is easily remedied by adjusting the incremental time step according to $\Delta t = \Delta\tau b/V$ and discretizing the structural model based on the new Δt. That is, if one leaves the V dependency in the structure,

$$\boldsymbol{A}_{d2} \equiv \begin{bmatrix}\boldsymbol{A} & \boldsymbol{B}\boldsymbol{C}_s\\ q\boldsymbol{B}_s(V)\boldsymbol{C} & \boldsymbol{A}_s(V) + q\boldsymbol{B}_s(V)\boldsymbol{D}\boldsymbol{C}_s\end{bmatrix} \tag{104}$$

then aeroelastic model II. becomes valid for all air speeds.

Results and Discussion

To demonstrate the proposed method, an unsteady vortex-lattice aerodynamic model subjected to several structural mode inputs is considered. It is mentioned that Refs. 13 and 14 also examined an aerodynamic model based on the vortex-lattice method for system identification by proper orthogonal decomposition (POD) and ERA methods. Both types of reduced-order aeroelastic models are constructed using the methods described in the preceding section. For simplicity of implementation, only the results from the SCI/ERA method with a sufficient number of output measurements are presented here. Occasionally, the alternative scheme with augmented output measurements was applied and indeed found to produce reduced-order models of essentially the same qualities as those presented here.

Unsteady flowfield around a flat, rectangular wing in incompressible, subsonic airflow is modeled by the vortex-lattice formulation (Fig. 3). The wing is 3 in. wide and 12 in. long, has 10 and 20 vortex elements in the chordwise and spanwise directions, respectively. The free wake has 40 and 20 vortex elements in the streamwise and spanwise directions, creating a total of 800 degrees of freedom.[15] The

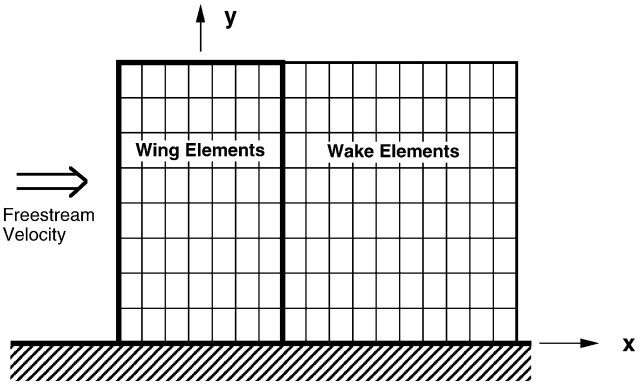

Fig. 3 Vortex-lattice grids for rectangular semispan.

wing structure is modeled by using six vibrational (three bending and three torsional) modes.[16] The natural vibration frequencies of these modes are 138.1, 649.6, 892.9, 2289.6, 2508.0, and 4160.2 rad/s, respectively. No structural damping was introduced at this time. Thus, the size of the full-order aeroelastic model is (812 × 812).

For the aeroelastic model I, the reference air density and speed were set at 1.23 kg/m^3, 80 m/s, respectively. The incremental time at this reference speed is $\Delta t = \mathrm{d}x/\mathrm{V}_{\mathrm{ref}} = 9.525 \times 10^{-5}$ s. For the sampling of the vortex model, 480 extra outputs were extracted in addition to the six generalized aerodynamic forces at 481 time steps. Applying 12 sets of random signal inputs simultaneously, six for $\boldsymbol{u}^n$, six for $\dot{\boldsymbol{u}}^n$, yielded a single set of sampled data. Twelve pulse inputs were also applied individually at the first two time steps to generate $\boldsymbol{Y}^0$ and $\boldsymbol{Y}^1$. Figure 4 shows three sequences of the random numbers generated on MATLAB®. Of 481 time samples, the SVD produced 413 linearly independent singular modes. This number was determined by the rank of $\boldsymbol{H}_{c0}$ matrix. Thus, the size of the aerodynamic ROM became (413 × 413). The reduced-order aerodynamic model was then coupled with the structural model to create (425 × 425) aeroelastic model (ROM I.).

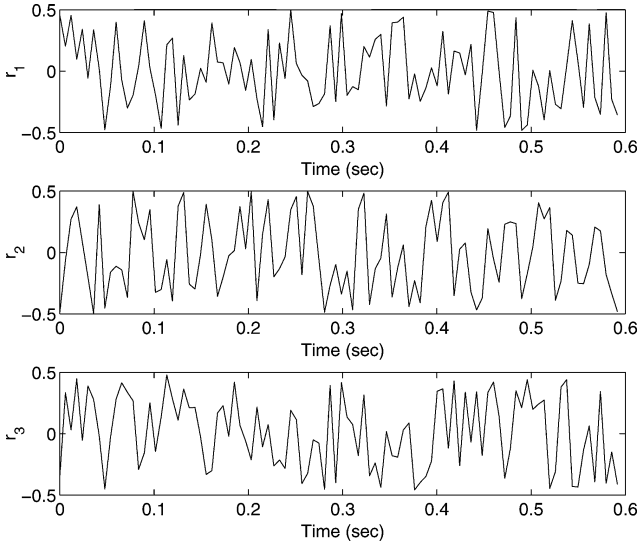

Fig. 4 Statistically independent random signals.

For aeroelastic model II, the reference air density and speed were again set at 1.23 kg/m^3 and 80 m/s. Six sets of random signals and six sets of discrete-time derivatives of the random signals were applied for $\boldsymbol{u}^n$ and $\dot{\boldsymbol{u}}^n$ using 481 time steps and the 486 output measurements. This yielded (329 × 329) aerodynamic ROM, which when combined with the structural system, produced (341 × 341) aeroelastic model (ROM II). ROM II is approximately 20 % smaller than ROM I as a result of using only the half of the input channels.

Next, the dimensions of the reduced-order aerodynamic models were further decreased using the FDKL/SCI method. As mentioned earlier, the incremental time step embedded in both the FOM and SCI/ERA ROM is too small to be effective for various aeroelastic simulations, which usually involve a low-frequency range. Considering that the highest free vibration frequency of the structural modes is 4160 rad/s, the sampling range in the FDKL method was restricted to (−4500, 4500) rad/s. For the ROM I, of 174 frequency samples within the range, 129 KL modes were selected based on the rank of the covariance matrix $\boldsymbol{K}$. Hence, the size of the new reduced-order aerodynamic and aeroelastic models (ROM I-FDKL) became 129 and 141, respectively. Likewise, for the ROM II 97 KL modes of 130 frequency samples in the same frequency range were selected yielding a new (109 × 109) aeroelastic model (ROM II-FDKL). For computational efficiency, these reduced-order models are to be preferred over the ROM I and ROM II.

Figure 5 presents (6 × 6) generalized aerodynamic forces obtained from the FOM, ROM I-FDKL, and ROM II-FDKL, in the nondimensional time domain. It is seen that despite the cutoff frequency range present in the latter two models they reproduce the pulse aerodynamic responses of the original model very well.

Figures 6 and 7 show two different scales of the aeroelastic eigenvalues of the various models in the Laplace domain at $V = 80$ m/s. It is seen that many eigenvalues of the reduced-order aeroelastic models match very well with those of the full model (Fig. 6). More specifically, the 12 complex eigenvalues associated with six structural modes agree very well between the FOM and ROMs, although the higher structural modes (fifth and sixth) in the ROM II and ROM II-FDKL are slightly mismatched (Fig. 7). All of the eigenvalues of the ROM I-FDKL and ROM II-FDKL are approximately within the specified bound, (− 4500, 4500) rad/s. Presented in Figs. 8 and 9 are time responses of the first two structural modes caused by an initial condition in $\dot{u}_1$. It can be seen that the three sets of curves are practically indistinguishable from each other. The next set of

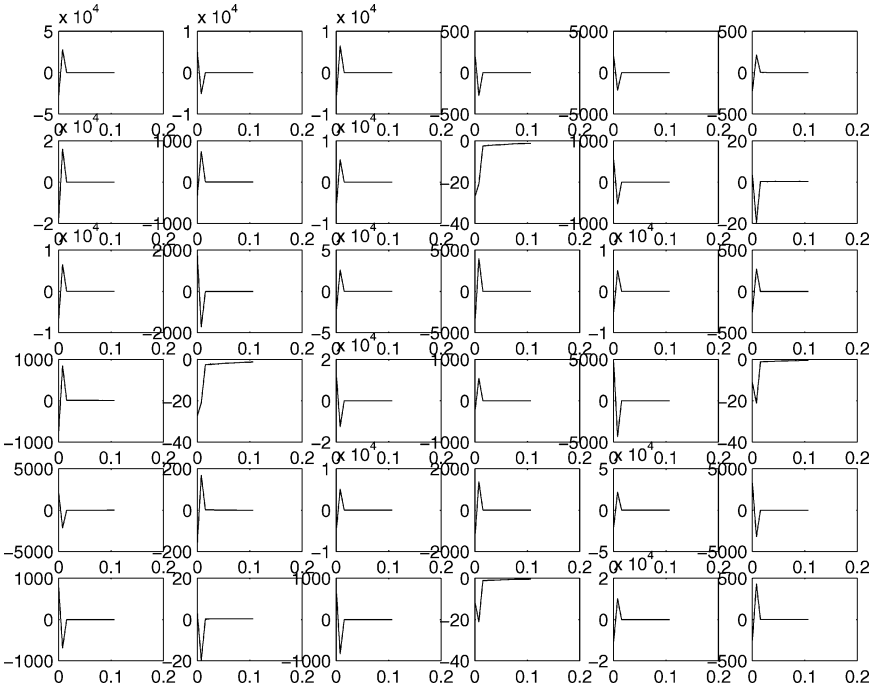

Fig. 5 (6 × 6) generalized aerodynamic forces at $V = 80$ m/s [- FOM (800) - - ROM I-FDKL (129) . . . ROM II-FDKL (97)].

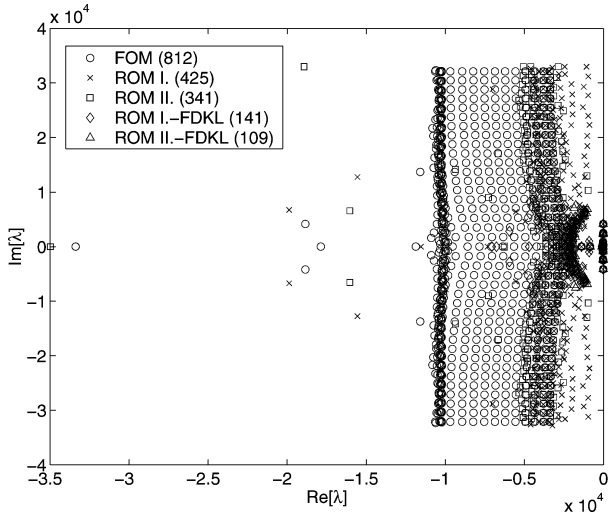

Fig. 6 Aeroelastic eigenvalues at $V = 80$ m/s.

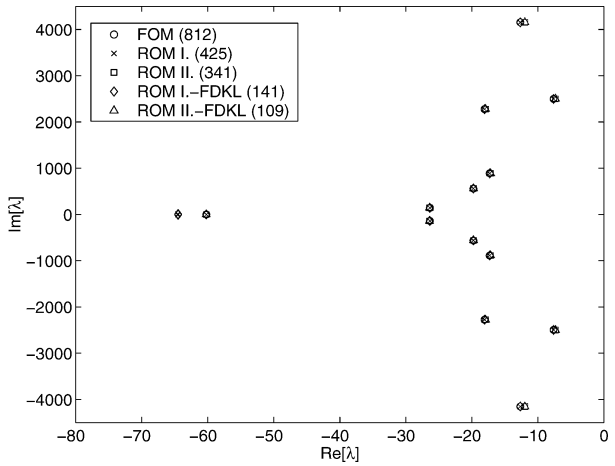

Fig. 7 Aeroelastic eigenvalues at $V = 80$ m/s (close-up).

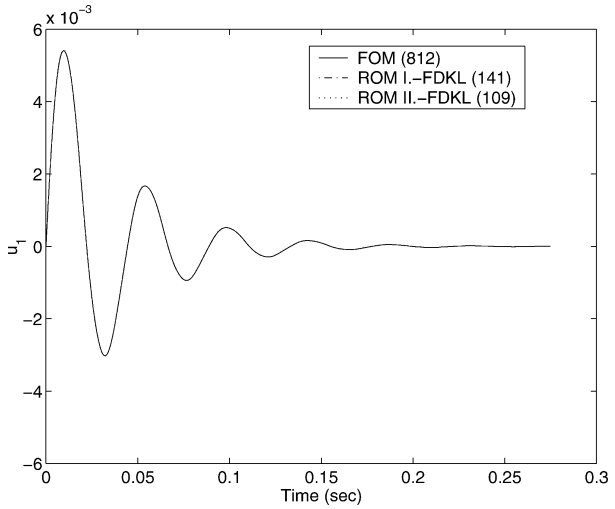

Fig. 8 Mode 1 aeroelastic response to initial condition (IC) in mode 1 at $V = 80$ m/s.

figures, Figs. 10–13 show aeroelastic results at $V = 121.2$ m/s. As can be seen, the wing is on the verge of flutter at this speed. Note how accurately the ROM I-FDKL is able to reproduce neutrally stable, sinusoidal time responses (Figs. 12 and 13). However, the ROM II-FDKL exhibits a noticeable but minor error in producing the transient responses.

Finally, the model construction time is compared between the pulse/ERA and SCI/ERA methods. To obtain accurate and

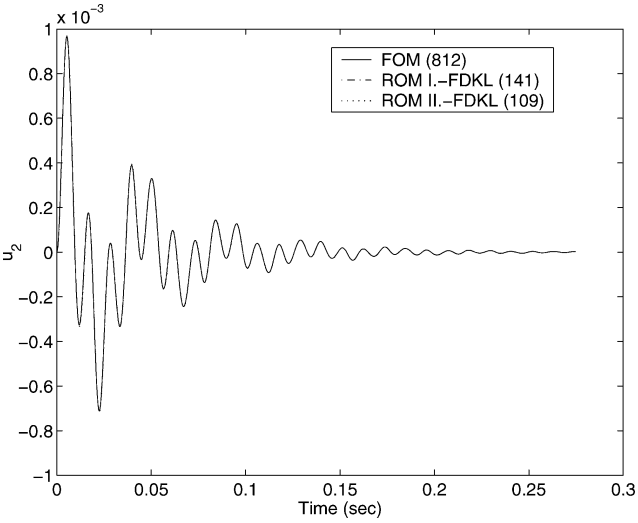

Fig. 9 Mode 2 aeroelastic response to IC in mode 1 at $V = 80$ m/s.

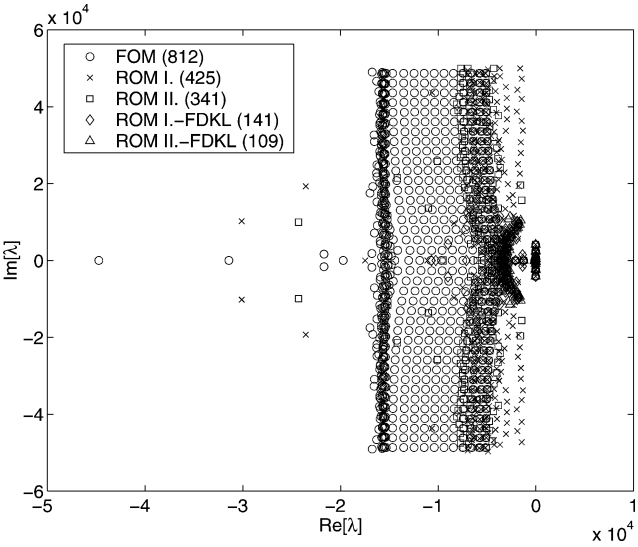

Fig. 10 Aeroelastic eigenvalues at $V = 121.2$ m/s.

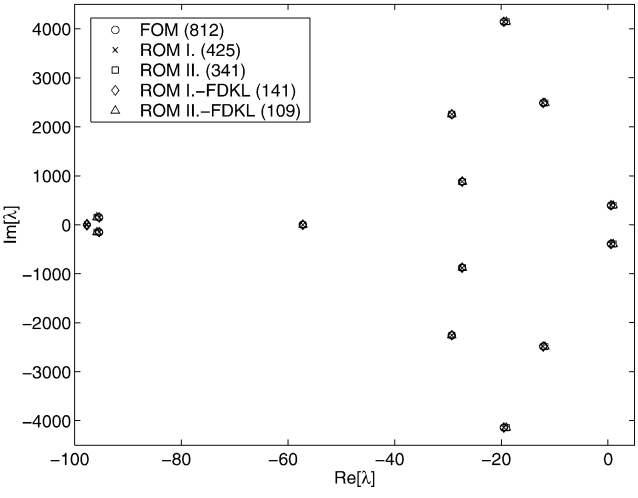

Fig. 11 Aeroelastic eigenvalues at $V = 121.2$ m/s (close-up).

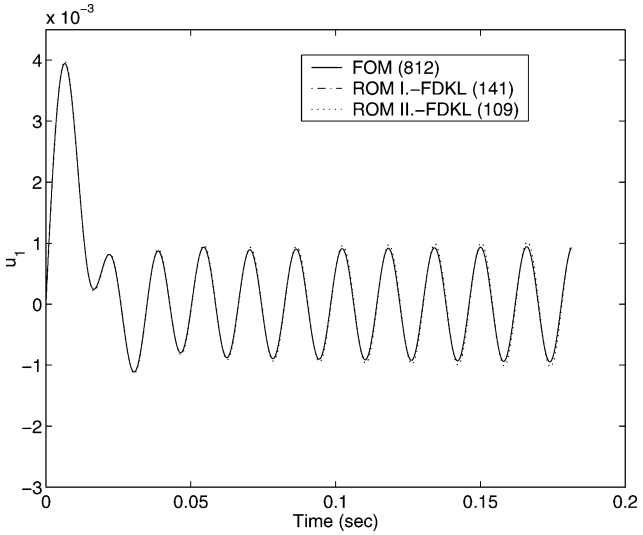

Fig. 12 Mode 1 aeroelastic response to IC in mode 1 at $V = 121.2$ m/s.

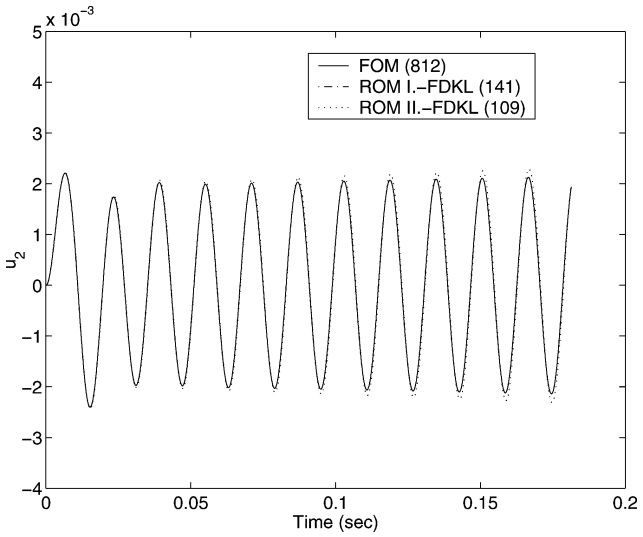

Fig. 13 Mode 2 aeroelastic response to IC in mode 1 at $V = 121.2$ m/s.

consistent singular modes, $\boldsymbol{H}_{c0}, \boldsymbol{H}_{c1}$ matrices were kept as square as possible by keeping the number of time samples approximately equal to the total number of measurements, which is the sum of the number of generalized aerodynamic forces and the number of auxiliary measurements. The same numbers of time steps and auxiliary outputs were used in both algorithms. Thus, in the first case where only the first bending mode alone excited the flowfield, $M = 131$, $N_o = 131$. In the second case where the first bending and first torsional modes were included, $M = 251$, $N_o = 252$, and in the third case where the first bending and torsional as well as the second bending modes excited the aerodynamic field, $M = 281$, $N_o = 283$. Four and five inputs were also used with $M = 331$, $N_o = 334$, and $M = 411$, $N_o = 415$, respectively. Table 1 shows CPU seconds spent in constructing ROM I on a Silicon Graphics, Inc. (SGI) machine. Also presented in parenthesis are the dimensions of the corresponding reduced-order models. Table 2 shows CPU seconds consumed for ROM II on the SGI machine. Presented again in Fig. 14 is the CPU seconds vs the number of inputs for ROM I and ROM II. Note that these numbers represent total CPU seconds spent not only in sampling the response but also processing the data in the subsequent ERA schemes. As seen from the tables and figure, the new method clearly has an advantage over the pulse/ERA in reducing the model construction time yielding saving factors of multiple numbers. Needless to say, as the number of inputs increases, so does the saving. For a given number of inputs, both ERA methods generate

Table 1 Comparison of CPU time for ROM I

No. of inputs	Pulse/ERA, s	SCI/ERA, s
1	12.3 (92)[a]	6.7 (89)[a]
2	74.8 (180)	16.6 (182)
3	150.8 (221)	20.6 (226)
4	327.8 (297)	28.2 (298)
5	762.3 (336)	43.7 (340)
6	1525.5 (395)	63.2 (413)

[a]Number in parentheses is the size of ROM.

Table 2 Comparison of CPU time for ROM II

No. of inputs	Pulse/ERA, s	SCI/ERA, s
1	6.3 (92)[a]	6.8 (89)[a]
2	32.8 (169)	17.00 (167)
3	65.9 (215)	21.0 (214)
4	130.1 (258)	27.6 (257)
5	279.6 (304)	44.1 (305)
6	540.4 (316)	61.4 (329)

[a]Number in parentheses is the size of ROM.

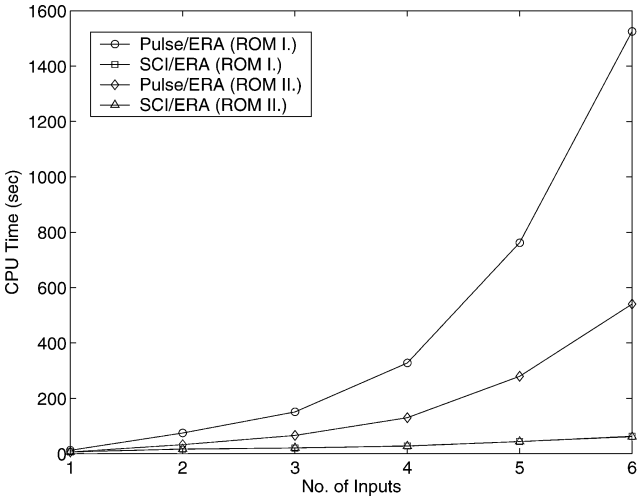

Fig. 14 Model construction time of vortex lattice ERA ROMs vs number of inputs.

ROMs of very similar sizes. As expected, ROM II of the SCI/ERA are as small as 80% of the corresponding ROM I. Despite the different input channels, both SCI/ERA ROM I and ROM II require approximately the same CPU time, implying that in the SCI/ERA the overall computation time is not very sensitive to the number of inputs.

Conclusions

In this paper, an efficient time-domain system identification and model reduction technique for linear dynamic systems that are subjected to multiple right-hand-side inputs has been presented and demonstrated. The method is a postprocessing procedure that does not require modifying the original code and takes only input and output data for the model construction. The new method is based on the direct singular value decomposition of output measurements that are not necessarily attributed to pulse inputs but caused by multiple signal inputs applied simultaneously at the input channels. Compared to the pulse/ERA, the SCI/ERA can significantly reduce the model construction time and compress the amount of output data. Therefore, it is very attractive for large-scaled dynamic systems with multiple driving inputs such as CFD models wherein the moving boundary input is often described by many structural modes. For practical applications a second model reduction of the ERA ROM is desirable. For this purpose, the FDKL/SCI method is recommended for its efficiency and accuracy. Although not presented in this paper, for best performance of the new algorithm one could further

optimize the number of time steps based on rank updating of the data matrices, an algorithm that is adopted in the aforementioned FDKL/SCI method.

Acknowledgments

The author is grateful to his former manager, Steven R. Precup, and Senior Technical Fellow Kumar G. Bhatia for their continuous support for this research.

References

[1]Juang, J.-N., *Applied System Identification*, Prentice–Hall, Englewood Cliffs, NJ, 1994, Chap. 5.

[2]Silva, W. A., and Bartels, R. E., "Development of Reduced-Order Models for Aeroelastic Analysis and Flutter Prediction Using CFL3Dv6.0 Code," AIAA Paper 2002-1596, April 2002.

[3]Hong, M. S., Bhatia, K. G., SenGupta, G., Kim, T., Kuruvila, G., Silva, W. A., Bartels, R., and Biedron, R., "Simulations of a Twin-Engine Transport Flutter Model In the Transonic Dynamics Tunnel," International Forum on Aeroelasticity and Structural Dynamics, IFASD Paper 2003-US-44, June 2003.

[4]Dowell, E. H., Hall, K. C., and Romanowski, M. C., "Eigenmode Analysis in Unsteady Aerodynamics; Reduced-Order Models," *Applied Mechanics Review*, Vol. 50, No. 6, 1997, pp. 371–386.

[5]Kim, T., "An Efficient Response-Based Modal Analysis for Dynamic Systems with Multiple Inputs," AIAA Paper 2001-1380, April 2001.

[6]Kim, T., and Bussoletti, J. E., "An Optimal Reduced-Order Aeroelastic Modeling Based on a Response-Based Modal Analysis of Unsteady CFD Models," AIAA Paper 2001-1525, April 2001.

[7]Hall, K. C., "Eigenanalysis of Unsteady Flows About Airfoils, Cascades, and Wings," *AIAA Journal*, Vol. 32, No. 12, 1994, pp. 2426–2432.

[8]Ho, B. L., and Kalman, R. E., "Effective Construction of Linear State-Variable Models from Input/Output Functions," *Regelungstechnik*, Vol. 14, No. 12, 1966, pp. 545–548.

[9]Juang, J.-N., and Pappa, R. S., "An Eigensystem Realization Algorithm for Modal Parameter Identification and Model Reduction," *Journal of Guidance, Control, and Dynamics*, Vol. 8, No. 5, 1985, pp. 620–627.

[10]Kim, T., Hong, M. S., Bhatia, K. G., and SenGupta, G., "Aeroelastic Model Reduction for an Affordable CFD Based Flutter Analysis," AIAA Paper 2004-2040, April 2004; also *AIAA Journal* (submitted for publication).

[11]Kim, T., "Frequency-Domain Karhunen-Loeve Method and Its Application to Linear Dynamic Systems," *AIAA Journal*, Vol. 36, No. 11, 1998, pp. 2117–2123.

[12]Kim, T., "Discrete-Time Eigen Analysis and Optimal Model Reduction for Flutter and Aeroelastic Damping/Frequency Prediction Based on CFL3D-ERA," The Boeing Co., B-ADVTECH-LLL-M02-013, BCAG, Seattle, WA, Feb. 2003.

[13]Juang, J.-N., Kholodar, D., and Dowell, E. H., "System Identification of a Vortex Lattice Aerodynamic Model," *AIAA Journal*, Vol. 40, No. 6, 2002, pp. 1187–1196.

[14]Tang, D., Kholodar, D., Juang, J.-N., and Dowell, E. H., "System Identification and Proper Orthogonal Decomposition Method Applied to Unsteady Aerodynamics," *AIAA Journal*, Vol. 39, No. 8, 2001, pp. 1569–1576.

[15]Kim, T., Nam, C., and Kim, Y., "Reduced-Order Aeroservoelastic Model with an Unsteady Aerodynamic Eigen Formulation," *AIAA Journal*, Vol. 35, No. 6, 1997, pp. 1087, 1088.

[16]Crawley, E. F., and Dugundji, J., "Frequency Determination and Non-Dimensionalization for Composite Cantilever Plates," *Journal of Sound and Vibration*, Vol. 72, No. 1, 1980, pp. 1–10.

A. Berman
Associate Editor